Title
Early-Age Temperature Development in Concrete Pavements Containing Microencapsulated Phase Change Materials

Author
SHE, ZHENYU

Publication Date
2018

Peer reviewed|Thesis/dissertation

UNIVERSITY OF CALIFORNIA
Los Angeles

Early-Age Temperature Development in Concrete Pavements Containing Microencapsulated Phase Change Materials

A thesis submitted in partial satisfaction
of the requirements for the degree
Master of Science in Mechanical Engineering

by

Zhenyu She

2018

ABSTRACT OF THE THESIS

Early-Age Temperature Development in Concrete Pavements Containing Microencapsulated Phase Change Materials

by

Zhenyu She
Master of Science in Mechanical Engineering
University of California, Los Angeles, 2018
Professor Laurent G. Pilon, Chair

This study investigates experimentally and numerically the addition of microencapsulated phase change materials (PCMs) into concrete pavements at early ages to limit (i) temperature rise caused by cement-water hydration, (ii) cooldown rate, and (iii) the associated risk of thermal cracking. First, the effect of water-reducing admixture (WRA) on the heat generation rate from cement hydration was quantified using isothermal calorimetry. Second, large cubic PCM-mortar composite specimens representative of a common pavement geometry were prepared and placed in an environmental test chamber simulating realistic diurnal conditions. The results showed that the presence of PCM can reduce considerably the temperature rise and cooldown rate across the cementitious composite section within the first 24 hours following placement provided the PCM melting temperature is selected carefully. This was in spite of the fact that the lower thermal conductivity of PCM-composites inhibited heat dissipation. A transient 1D thermal model of pavement section was developed to simulate the temperature evolution and the rate of change in temperature within PCM-mortar composite sections. Good agreement was found between model predictions and experimental measurements. In addition, a parametric study was carried out to assess the effects of the PCM melting characteristics (temperature, temperature window, latent heat) on local temperature in PCM-mortar composites. The constitutive relationships and the numerical model developed as part of this study can be used to inform the design of concrete pavements containing PCMs for early-age crack resistance.

The thesis of Zhenyu She is approved.

Adrienne G. Lavine

Gaurav Sant

Laurent G. Pilon, Committee Chair

University of California, Los Angeles

2018

TABLE OF CONTENTS

LIST OF FIGURES

LIST OF TABLES

NOMENCLATURE

C_c	cement content, kg/m^3
c_p	specific heat, J/kg K
f	objective function
h	convective heat transfer coefficient, W/m^2 K
h_{sf}	latent heat of fusion, kJ/kg
k	thermal conductivity, W/m K
L_c	height of PCM-mortar composite slab, m
L_s	steel plate thickness, m
$\dot{q}(t)$	volumetric heat generation rate, W/m^3
$\dot{q}_g(t)$	heat generation rate per unit mass of cement, W/kg
$Q(t)$	cumulative volumetric heat generated, J/m^3
$Q_g(t)$	cumulative heat generated per unit mass of cement, J/kg
t	time, s or h
t_{eq}	equivalent time, s or h
$T(x,t)$	temperature at location x and time t, °C
T_{pc}	PCM phase change temperature, °C
ΔT_{pc}	PCM phase change temperature window, °C
T_{ref}	reference temperature, °C
T_{max}	maximum temperature of PCM-mortar composite slab, °C
T_{min}	minimum temperature of PCM-mortar composite slab, °C
w/c	water/cement ratio
x	distance from the bottom of PCM-mortar composite slab, m

Greek symbols

ρ	density, kg/m^3
ϕ_j	volume fraction of material "j" in composite
τ	oscillation period, h

Subscripts

c	refers to PCM-mortar composite slab
co	refers to the core of PCM capsule
eff	refers to effective properties
m	refers to cement paste in composite
mo	refers to cement mortar in composite
pcm	refers to phase change material
q	refers to quartz sand
s	refers to steel plate
sh	refers to the shell of PCM capsule
w	refers to water in the water bath
∞	refers to air in the chamber

CHAPTER 1

Introduction

After mixing and placement of concrete pavement, heat generation from cement-water hydration reactions causes temperature to rise and leads to spatial temperature gradients within the pavements [2, 3]. Assuming proper design, placement, and curing, the two major causes of early-age cracking are thermal strain and autogenous shrinkage [4]. Several methods have been developed to mitigate thermal cracking including modifying the mixture proportions and replacing cement with mineral admixtures (e.g., fly ash, silica fume, and slag) [5]. Adding shrinkage-reducing admixtures and utilizing internal curing can also alleviate autogenous shrinkage [6, 7]. Other direct methods, such as using ice water for cement hydration, can also reduce the temperature at early ages [8].

Adding microencapsulated phase change materials (PCMs) into concrete has been recently proposed as an effective approach to limit the temperature rise of concrete at early ages [9–12]. PCMs are thermal energy storage materials that can store large amounts of latent heat associated with reversible melting and solidification processes [13, 14]. In order to avoid leakage of melted PCMs and prevent their reaction with the cement, PCMs are typically microencapsulated in polymeric shells with average diameter around 10 μm [15, 16] before being incorporated in cementitious materials. As heat is released by cement hydration, it is absorbed and stored in the form of latent heat of fusion in the microencapsulated PCMs. Then, the maximum temperature of the concrete and the corresponding temperature gradient at early ages are both reduced [3, 17], as well as the rate of temperature change. In addition, during cooling below the phase change temperature, the concrete temperature declines much more slowly due to the heat released by the solidification process. Thus, the cooldown rate is also reduced.

The present study aims (i) to determine the effect of WRA, microencapsulated PCMs, and quartz sand on the heat generation rate associated with cement hydration in PCM-mortar composite sections, (ii) to experimentally measure the temperature evolution and rate of temperature change within early-age concrete pavement sections containing various dosages of microencapsulated PCMs, (iii) to compare the measured temperature evolutions and rate of temperature change with numerical predictions from a 1D transient thermal model in order to validate the ability of such a model to accurately predict temperature development within fresh concrete pavements, (iv) to carry out a parametric study to assess the effects of the melting characteristics of microencapsulated PCMs on the local temperature evolution in PCM-mortar composites.

CHAPTER 2

Background

2.1 Early-age thermal cracking in concrete pavements

One of the promising applications of PCM-concrete composite is in road pavements and bridge decks. Indeed, the quality of American roads was given a grade of "D" by the American Society of Civil Engineers in 2017 [18]. A major contributor to road deterioration is thermal cracking in concrete pavements, which can be divided into two categories: (i) early-age thermal cracking and (ii) thermal fatigue cracking. Early-age cracking occurs as a result of exothermic hydration reactions between ordinary Portland cement (OPC) and water within the fresh concrete. Heat release from such reactions causes the internal temperature within the pavement sections to rise, leading to the development of thermal strains and stresses and possible crack formation. Figure 2.1 shows a photograph of a pavement section exhibiting early-age cracks.

The inclusion of microencapsulated PCMs into concrete has been suggested as a means of reducing early-age temperature rise and mitigating the corresponding cracking risk [9,10]. The PCM's latent heat can be exploited to absorb a portion of the heat released by cement hydration, thereby lowering the extent of temperature rise within the section. Furthermore, the heat is then released upon PCM solidification, slowing the rate of temperature decrease in the section to mitigate the risk of shrinkage cracking.

Figure 2.1: Typical early-age thermal cracking of the concrete pavement [1].

While the use of microencapsulated PCMs in concrete pavements is a promising approach to reducing cracking risk, such an application has yet to be rigorously explored. The effect of PCM dosage on early-age temperature rise in cementitious materials has been studied [3, 9, 10]. However, the thermal behavior of full-sized PCM-containing pavement sections exposed to realistic climate conditions has not been verified experimentally or further explored through modeling. It remains unclear how much of an effect the inclusion of PCMs has in reducing early-age temperature rise and cooldown rate within fresh pavement sections, and how this reduction in temperature rise or cooldown rate is influenced by the effective thermal properties of the PCM-concrete composite.

2.2 Thermal properties of PCM-mortar composites

The PCM-mortar composite considered in this study was a heterogeneous composite material consisting of spherical PCM microcapsules randomly distributed in a mortar matrix. It has been demonstrated that its transient thermal behavior is equivalent to that of a homogeneous material with some effective thermal properties [19, 20]. The effective thermal conductivity

k_{eff} of such composites can be predicted by the Felske's model, expressed as [21]

$$k_{eff} = \frac{k_{mo}(1-\phi_{co}-\phi_{sh})\left[6+4\frac{\phi_{sh}}{\phi_{co}}+2\frac{\phi_{sh}k_{co}}{\phi_{co}k_{sh}}\right]+(1+2\phi_{co}+2\phi_{sh})\left[(3+\frac{\phi_{sh}}{\phi_{co}}k_{co}+2\frac{\phi_{sh}}{\phi_{co}}k_{sh}\right]}{(2+\phi_{co}+\phi_{sh})\left[3+2\frac{\phi_{sh}}{\phi_{co}}+\frac{\phi_{sh}k_{co}}{\phi_{co}k_{sh}}\right]+(1-\phi_{co}-\phi_{sh})\left[(3+\frac{\phi_{sh}}{\phi_{co}})\frac{k_{co}}{k_{mo}}+2\frac{\phi_{sh}k_{sh}}{\phi_{co}k_{mo}}\right]} \tag{2.1}$$

where, ϕ_{co} and ϕ_{sh} are respectively the volume fractions of the PCM capsule core and shell, while k_{mo}, k_{co}, and k_{sh} are the thermal conductivities of the cement mortar, PCM capsule core and shell respectively. The validity of this expression has been demonstrated numerically [19] and validated experimentally [22]. The effective volumetric heat capacity of microencapsulated PCM-mortar composite can be evaluated as the volume-weighted average of the heat capacity of the different constituent materials [20],

$$(\rho c_p)_{eff}(T) = \phi_m(\rho c_p)_m + \phi_q(\rho c_p)_q + (1-\phi_m-\phi_q)(\rho c_p)_{pcm}. \tag{2.2}$$

Here, ϕ_m and ϕ_q are respectively the volume fractions of the cement paste and quartz sand, while $(\rho c_p)_m$, $(\rho c_p)_q$, and $(\rho c_p)_{pcm}$ are the volumetric heat capacities of the cement paste, quartz sand, and PCM, respectively. The specific heat capacity of PCM $c_{p,pcm}(T)$ can be described as a rectangular step function of temperature according to the effective heat capacity method [5],

$$c_{p,pcm}(T) = \begin{cases} c_{p,pcm,s} & T < T_{pc} - \Delta T_{pc}/2 \\ c_{p,pcm,s} + \frac{h_{sf}}{\Delta T_{pc}} & T_{pc} - \Delta T_{pc}/2 \le T \le T_{pc} + \Delta T_{pc}/2 \\ c_{p,pcm,l} & T > T_{pc} + \Delta T_{pc}/2 \end{cases} \tag{2.3}$$

where $c_{p,pcm,s}$ and $c_{p,pcm,l}$ are the specific heat capacity of the PCM in the solid and liquid phases, respectively, h_{sf} is the latent heat of fusion (in J/kg), T_{pc} is the PCM melting temperature, and ΔT_{pc} is the melting temperature window, over which phase change occurs. The effective heat capacity method has been shown to predict temporal evolution of temperature in PCM-mortar composites similar to those obtained using (i) experimentally measured $c_{p,pcm}(T)$ and (ii) its Gaussian fit which is more representative of behavior observed [23].

2.3 Thermal modeling of PCM-mortar composites

Šavija *et al.* [24] developed numerical models to predict the temperature and stress distribution in wall-on-slab systems. They confirmed that the addition of microencapsulated

PCMs has great potential in reducing temperature and stresses in hardening massive concrete structures. Arora *et al.* [17] conducted numerical simulations to study both the early-age and late-age thermal response of concrete pavements containing microencapsulated PCMs under environmental conditions. Early-age simulations demonstrated significant reductions in peak hydration temperature and heating/cooling rates when microencapsulated PCMs are incorporated in concrete, either as a partial replacement of the cement paste or as fine aggregates. This resulted in reduced cracking probabilities [17, 24, 25]. Simulations on mature pavements indicated temperature and curling stress reductions when appropriate PCMs were used. Finally, we conducted a parametric study on microencapsulated PCMs and numerically verified that adding PCMs, with properly selected thermal properties, to concrete pavement section could limit temperature rise due to exothermic cement hydration reactions and environmental exposure at early ages [3]. However, to the best of our knowledge, previous numerical simulations have not been validated experimentally. In addition, they made several simplifying assumptions that are not always satisfied in practice. For example, experimentally different dosages of water-reducing admixture (WRA) must be added to the cement formulation along with the microencapsulated PCMs in order to maintain adequate workability. These admixtures tend to delay the cement-water hydration reaction and the associated heat generation [26,27]. However, the presence and effects of admixtures have not been considered in terms of their effects on heat generation rate and temperature evolution within the concrete.

2.4 Heat generation rate in early-age PCM-mortar composites

Modeling the heat generation rate caused by cement-water hydration reactions is essential in predicting temperature evolution in fresh concrete. The equivalent age, or maturity method, has been widely used in the concrete industry to describe the progress of hydration reactions in cementitious materials [3,28,29]. The equivalent age $t_{eq}(x,t)$ can be expressed as a function of time and temperature history at a given location, i.e. [30],

$$t_{eq}(x,t) = \int_0^t \exp\left[-\frac{E_a}{R}\left(\frac{1}{T_c(x,t)} - \frac{1}{T_{ref}}\right)\right] \mathrm{d}t \tag{2.4}$$

where E_a (in kJ/mol) is the activation energy, $R = 8.314$ J/mol K is the ideal gas constant, T_{ref} is the reference temperature, in K. Then, the local heat generation rate $\dot{q}(x,t)$ (in W/m^3) during the hydration process can be expressed as a function of equivalent age t_{eq} [3, 28],

$$\dot{q}\left(x,t\right) = \frac{\mathrm{d}Q\left(t_{eq}\right)}{\mathrm{d}t_{eq}} \times \frac{\mathrm{d}t_{eq}}{\mathrm{d}t} = \dot{q}\left(t_{eq}\right) \times \exp\left[-\frac{E_a}{R}\left(\frac{1}{T_c\left(x,t\right)} - \frac{1}{T_{ref}}\right)\right] \tag{2.5}$$

where $Q(t_{eq})$ is the cumulative volumetric thermal energy released as a function of equivalent age, and $\dot{q}(t_{eq})$ is the heat generation rate as a function of equivalent age. Both of these quantities are determined from isothermal calorimetry measurements at a given reference temperature T_{ref} [3].

CHAPTER 3

Experiments

3.1 Materials and methods

3.1.1 Mixture proportions for PCM-mortar composites

In this study, four cementitious composite specimens (38 cm × 38 cm × 38 cm) were prepared with the following mixture proportions: (1) a plain mortar consisting of 45 vol.% cement paste and 55 vol.% quartz inclusions, (2) a microencapsulated PCM-mortar composite consisting of 45 vol.% cement paste, 45 vol.% quartz, and 10 vol.% MPCM24D (Microtek Laboratories, Inc.) with melting temperature $T_{pc} \simeq 24°C$ and latent heat of fusion $h_{sf} = 160$ kJ/kg, (3) a microencapsulated PCM-mortar composite consisting of 45 vol.% cement paste, 45 vol.% quartz, and 10 vol.% PCM35CP (Encapsys, LLC) with melting temperature $T_{pc} \simeq 35°C$ and latent heat of fusion $h_{sf} = 187$ kJ/kg and (4) a microencapsulated PCM-mortar composite consisting of 45 vol.% cement paste, 35 vol.% quartz, and 20 vol.% PCM35CP. The microencapsulated PCM consisted of a paraffin-based core material enclosed in melamine-formaldehyde (MF) shell. The cement paste was mixed using ASTM C150 [31] compliant Type I/II ordinary Portland cement (OPC) and deionized water with a water-cement ratio of 0.45 (mass basis) in accordance with ASTM C192 [32]. ASTM C778 [33] compliant graded quartz sand and microencapsulated PCM were used as inclusions within the cement mortar. Additionally, water-reducing admixture (WRA, MasterGlenium 7500, BASF Corporation) was added at different dosages based on the different mixture proportions to maintain adequate workability of the PCM-containing mortars. It was added at dosage of (i) 0.8% by mass of cement for Composition 1, (ii) 1.5% by mass of cement for Compositions 2 and 3, and (iii) 2.0% by mass of cement for Composition 4. Also, a viscosity-modifying admix-

ture (MasterMatrix VMA 450, BASF Corporation) was added at 260 ml/100 kg of cement to minimize segregation of inclusions and to maintain a homogeneous distribution of PCM microcapsules and quartz sand inclusions in all mortars. Table 3.1 summarizes the mixture proportions for these four PCM-mortar composite specimens. Finally, an evaporation retardant and finishing aid for concrete (MasterKure 111WB, BASF Corporation) was sprayed onto the top surface of the composite samples immediately after their placement to reduce water evaporation.

3.1.2 Isothermal calorimetry

In order to obtain the heat generation term $\dot{q}(t_{eq})$ given by Equation (2.5), an isothermal calorimeter (Tam Air, TA Instruments) was used to measure the volumetric thermal energy $Q(t_{eq})$ released and the corresponding heat generation rate $\dot{q}(t_{eq})$ within PCM-mortar composite specimens due to cement hydration for different mixture proportions. The measurements were performed for 7 days as described in ASTM C1702 [34]. The testing temperature of the isothermal calorimeter was set to the same reference temperature $T_{ref} = 298$ K. Reference specimens of DI water were prepared with equivalent total thermal capacity of the cementitious composites and used to measure the baseline heat flow signal. The baseline signal was subtracted from the measured heat flow of the cementitious composites. All mixture ingredients were conditioned to the testing temperature before mixing. Immediately after mixing, approximately 10 g of each sample was loaded into a 20 mL glass ampoule, sealed, and placed into the calorimeter. Table 3.2 summarizes the compositions of six different mortar samples synthesized to measure $\dot{q}(t_{eq})$ by isothermal calorimetry. The WRA used in these calorimetric experiments was the same as in the four cementitious specimens (i.e., MasterGlenium 7500, BASF Corporation), classified as Type A or Type F WRA in ASTM standard C494/C494M [35].

Table 3.1: Mixture proportions of the four PCM-mortar composite specimens placed in the experimental apparatus.

Specimen	Cement paste (vol.%)	ASTM quartz sand (vol.%)	Microencapsulated PCM (vol.%)	Water-cement ratio (%)	WRA (wt.% cement)	VMA 450 (ml/kg of cement)
1	45	55	0	45	0.8	2.6
2	45	45	10 (MPCM24D)	45	1.5	2.6
3	45	45	10 (PCM35CP)	45	1.5	2.6
4	45	35	20 (PCM35CP)	45	2.0	2.6

Table 3.2: Mixture proportions of the six PCM-mortar composite samples used to measure heat generation rate by isothermal calorimetry.

Sample	Cement paste (vol.%)	ASTM quartz sand (vol.%)	MPCM24D (vol.%)	Water-cement ratio (%)	WRA (wt.% cement)
1	100	0	0	45	0
2	100	0	0	45	0.8
3	90	0	10	45	0
4	90	0	10	45	0.8
5	90	10	0	45	0
6	90	10	0	45	0.8

3.2 Experimental methodology

3.2.1 Experimental test section

Figure 3.1a shows a schematic of the experimental test section used to measure transient temperature evolutions within representative PCM-mortar composite sections. The test section, in which the different mortars were cast, consisted of a formwork (interior dimensions: 38 cm × 38 cm × 38 cm) with 1.9 cm thick acrylic side walls and 0.6 cm thick stainless steel plate at the bottom. The height of 38 cm (15 inches) was selected to represent the thickness of a pavement section. To reproduce typical environmental conditions, the test section was placed in a programmable environmental chamber (TH024, Darwin Chambers Company) where it was subjected to a sinusoidal air temperature profile. In addition, a constant temperature was imposed at the bottom surface of the pavement section thanks to a circulating water bath (10 cm × 38 cm × 38 cm) flowing under the stainless steel plate to simulate the constant temperature of the subgrade. Polyurethane foam panels 4.8 cm in thickness were placed on each vertical side of the box to minimize heat losses.

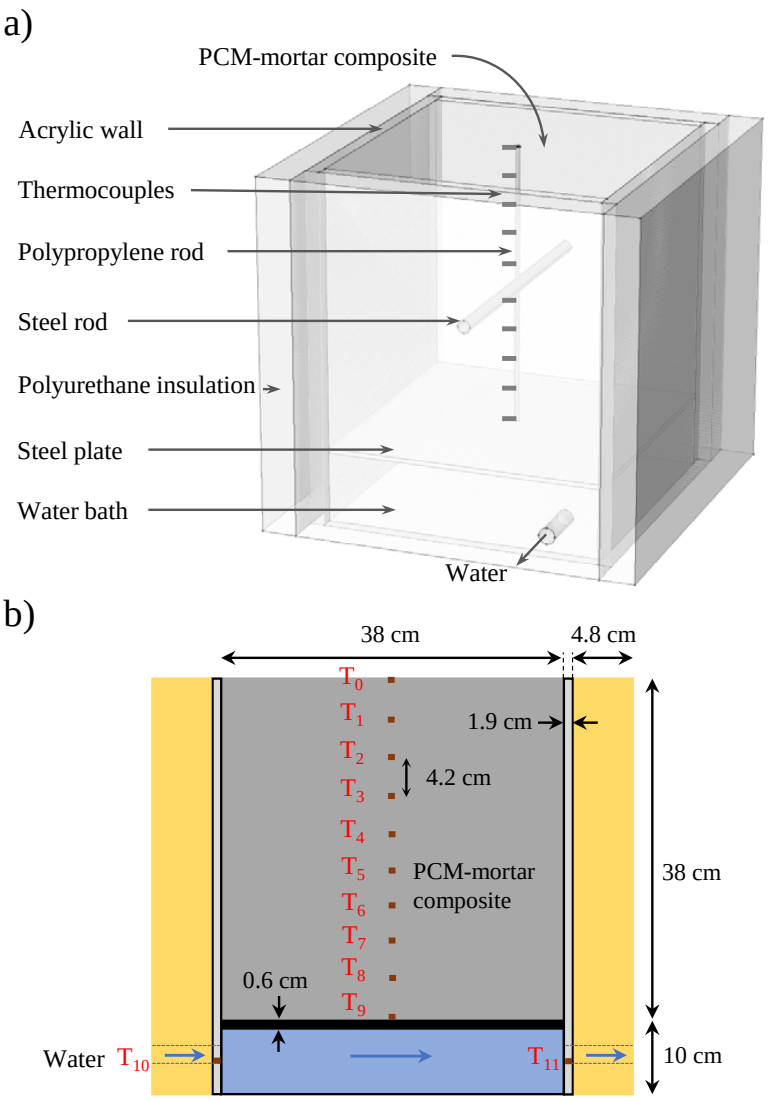

Figure 3.1: (a) Schematic of the experimental apparatus with internal dimensions 38 cm × 38 cm × 38 cm. The formwork was made of 1.9 cm thick acrylic while the outside foam was 4.8 cm thick polyurethane. A circulating water bath with dimensions 10 cm × 38 cm × 38 cm was set at the bottom. (b) Sectional view of the experimental apparatus with geometric dimensions.

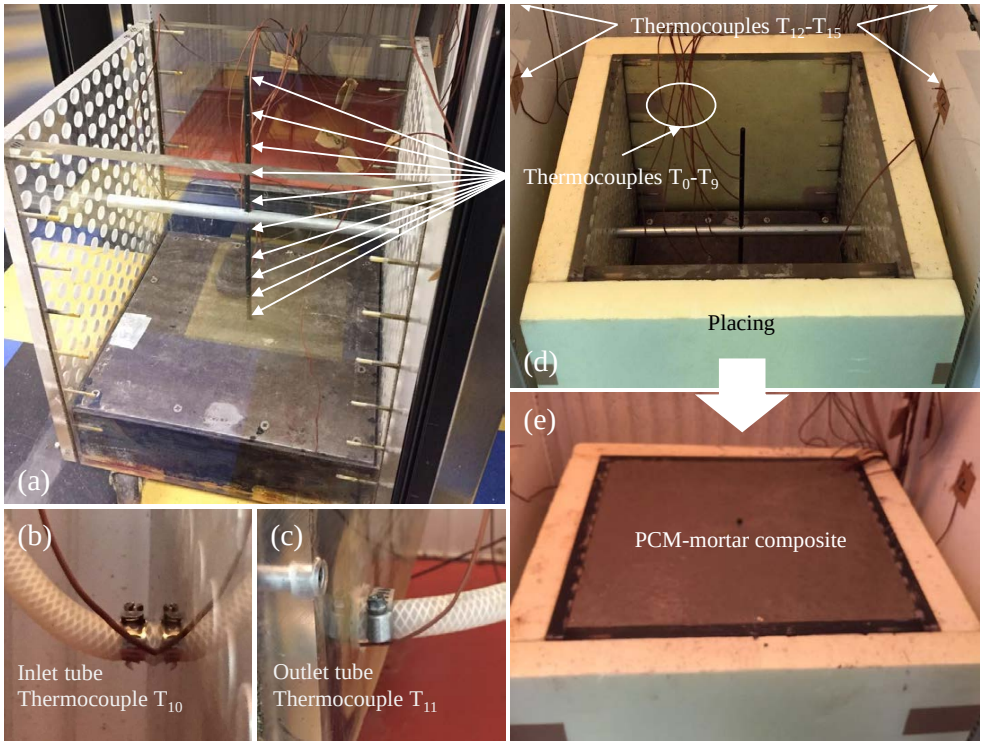

Figure 3.2: Photographs of the experimental apparatus and thermocouple placement. (a) Ten thermocouples T_0 - T_9 were evenly placed along a vertical polypropylene rod supported by a horizontal steel rod. Thermocouples T_{10} and T_{11} were inserted into (b) the inlet and (c) the outlet tubes of water bath. (d) Four thermocouples T_{12} - T_{15} were pasted on the inside walls of the environmental chamber. (e) Overview of a PCM-mortar composite specimen placed in experimental apparatus.

The temperature at the centerline of the pavement section was measured via 10 type-T thermocouples, denoted by T_0 to T_9, evenly distributed along the vertical direction, as illustrated in Figure 3.1. The thermocouples were attached to a supporting vertical polypropylene rod (0.8 cm OD, 0.3 cm ID) passing through the center of a horizontal steel rod (1.8 cm OD, 1.6 cm ID) for structural support. Both the vertical and horizontal bars were as thin as possible to minimize their effect on the temperature development within the composite sections while still providing sufficient support to maintain the thermocouples in their desired position. The inlet and outlet temperatures of the water bath were monitored by two type-T thermocouples denoted by T_{10} and T_{11}, respectively. The chamber temperature

was also monitored by four type-T thermocouples T_{12} to T_{15}. The type-T thermocouples were connected to 16-channel input modules (NI 9213, National Instruments) in a compact DAQ chassis (cDAQ-9178, National Instruments). Each input module provided built-in cold-junction compensation. Data acquisition was facilitated by LabVIEW 2014. Figure 3.2 shows photographs of the experimental apparatus including (a) thermocouple placement within the test section, (b) inlet and (c) outlet pipes, and (d) the inside of chamber without and (e) with the PCM-mortar composite.

3.2.2 Experimental uncertainty analysis

During each experiment, the temperature of the environmental chamber was controlled within ± 0.2°C, and temperature throughout the chamber was expected to vary by no more than 1°C among different locations. The maximum uncertainty in thermocouple temperature measurements was about ± 0.5°C based on the calibration procedure performed using a refrigerating/heating circulator (AD28R-30-A11B, PolyScience) between 5 and 70°C. The uncertainty in the thermocouple locations was on the order of ± 3 mm, and the corresponding temperature error caused by the uncertainty in location was less than ± 0.2°C according to numerical simulation results.

3.2.3 Experimental procedures

The PCM-mortar composites described previously were cast into the cubic acrylic mold shown in Figure 3.2. After placement of the composites, all temperature measurements were recorded as a function of time for 28 days. The water temperature, set to 20°C, was controlled by the refrigerating/heating circulator previously used for thermocouple calibration. Figure 3.3a shows the inlet and outlet temperatures of the water bath for the first 24 hours. The temperature difference between inlet and outlet was less than 1°C throughout the duration of the test. Thus, the water temperature could be treated as constant.

Each PCM-mortar specimen was placed in the environmental chamber and subjected to sinusoidal temperature cycles with period $\tau = 24$ hours with minimum and maximum of

10°C and 40°C, respectively, such that the chamber temperature $T_\infty(t)$ was given by

$$T_\infty(t) = 15 \sin\left(\frac{\pi}{12}t\right) + 25°\text{C} \tag{3.1}$$

where t is in hours. The chamber temperature was measured at four different locations in the environmental chamber to confirm that it was uniform as illustrated in Figure 3.3b.

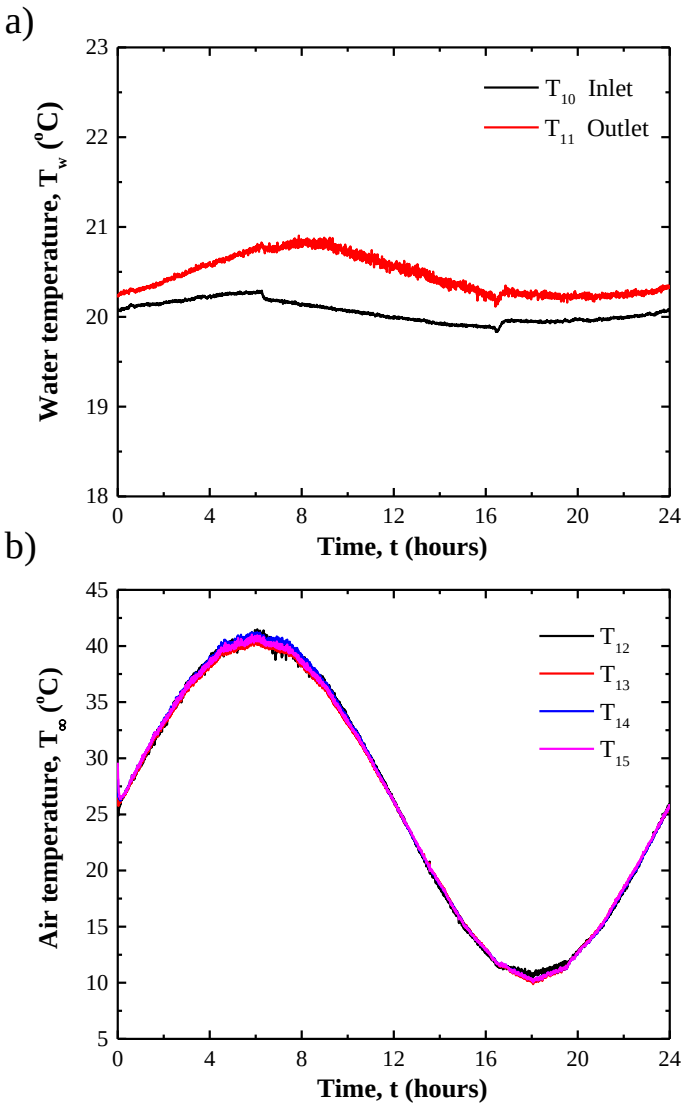

Figure 3.3: (a) Inlet and outlet temperatures of the water bath T_{10}, T_{11} as functions of time for one day. (b) Temperature of air in the chamber T_{12} - T_{15} for one day.

CHAPTER 4

Numerical Modeling

4.1 Schematic and assumptions

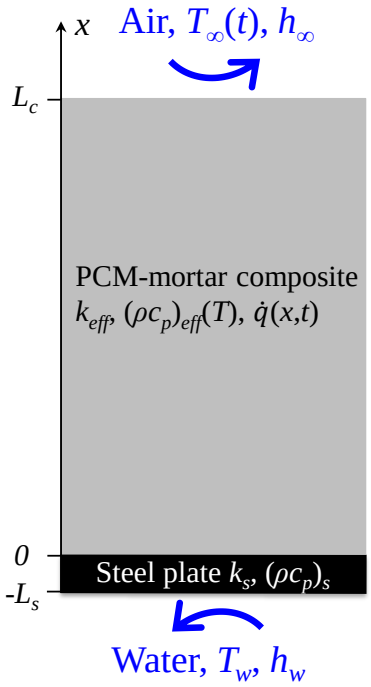

Figure 4.1: Schematic of the 1D thermal model of the homogeneous PCM-mortar composite of thickness L_c with effective thermal properties k_{eff} and $(\rho c_p)_{eff}$ placed over a steel plate (k_s and $(\rho c_p)_s$) cooled by water at temperature T_w.

Figure 4.1 illustrates the simulated 1D domain of the experimental test section. The PCM-mortar composite section was treated as homogeneous with effective thermal conductivity

k_{eff} and volumetric heat capacity $(\rho c_p)_{eff}(T)$ and subjected to a local heat generation rate per unit volume $\dot{q}(x,t)$. The upper surface of the pavement ($x = L_c$) experienced convective heat transfer with the air in the chamber at temperature $T_\infty(t)$ with convective heat transfer coefficient h_∞. The steel plate below the PCM-mortar composite specimen had a thermal conductivity k_s and volumetric heat capacity $(\rho c_p)_s$. The bottom surface of the steel plate ($x = 0$) experienced convective heat transfer with water at temperature T_w with convective heat transfer coefficient h_w.

The following assumptions were made to make the problem mathematically tractable: (i) the microencapsulated PCM-mortar composite behaved as a homogeneous medium with effective thermal properties k_{eff} and $(\rho c_p)_{eff}(T)$, (ii) all materials were isotropic with constant properties except for the PCM specific heat capacity which depended on temperature, (iii) the convective heat transfer coefficients h_∞ and h_w remained constant, and (iv) evaporative cooling at the specimen surface was negligible.

4.2 Governing equations

The temperature within the PCM-mortar composite section $T_c(x,t)$ was governed by the 1D transient heat diffusion equation with heat generation [36], i.e.,

$$(\rho c_p)_{eff}(T_c)\frac{\partial T_c}{\partial t} = k_{eff}\frac{\partial^2 T_c}{\partial x^2} + \dot{q}(x,t). \tag{4.1}$$

Here, $\dot{q}(x,t)$ is the local heat generation rate per unit volume expressed in W/m^3. Similarly, the temperature of the steel plate section $T_s(x,t)$ was governed by the 1D transient heat diffusion equation but without heat generation [36],

$$(\rho c_p)_s\frac{\partial T_s}{\partial t} = k_s\frac{\partial^2 T_s}{\partial x^2}. \tag{4.2}$$

4.3 Initial and boundary conditions

The mixing and placing processes were conducted at room temperature. Thus, the initial temperature of PCM-mortar composite and steel plate were equal to the room temperature

for each case, i.e.,

$$T_c\,(x,0) = T_s\,(x,0) = T_{room}. \tag{4.3}$$

Mixing each PCM-mortar uniformly took about half an hour. To account for the fact that cement hydration was already taking place during the mixing process before placement, the specimen was taken to be at an initial equivalent age of 0.5 h calculated from Equation (2.4), i.e.,

$$t_{eq}(x,0) = 0.5 \text{ h}. \tag{4.4}$$

Convective boundary conditions were applied both on the top surface of the PCM-mortar composite and at the bottom surface of the steel plate and expressed as,

$$-k_{eff}\,\frac{\partial T_c}{\partial x}\bigg|_{x=L_c} = h_\infty\left[T_c\,(L_c,t) - T_\infty\,(t)\right] \tag{4.5}$$

$$-k_s\,\frac{\partial T_s}{\partial x}\bigg|_{x=-L_s} = h_w\left[T_w - T_s\,(-L_s,t)\right]. \tag{4.6}$$

Finally, the temperature and heat flux were continuous across the interface of the PCM-mortar composite and the steel plate at all times, i.e.,

$$T_c\,(0,t) = T_s\,(0,t) \tag{4.7}$$

$$-k_{eff}\frac{\partial T_c}{\partial x}\,(0,t) = -k_s\frac{\partial T_s}{\partial x}\,(0,t). \tag{4.8}$$

4.4 Heat generation

According to Equation (2.5), the local heat generation rate $\dot{q}(x,t)$ from cement-water reactions at a given location can be expressed in terms of equivalent age $t_{eq}(x,t)$ and of the heat generation rate $\dot{q}(t_{eq})$ obtained from isothermal calorimetry. The heat generation rate $\dot{q}(t_{eq})$ can be expressed as the product of the cement content C_c (in kg/m^3) and the heat generation rate $\dot{q}_g(t_{eq})$ (in W/kg) per unit mass of cement [i.e., $\dot{q}(t_{eq}) = C_c\dot{q}_g(t_{eq})$], so that

$$\dot{q}\,(x,t) = C_c\dot{q}_g\,(t_{eq})\exp\left[-\frac{E_a}{R}\left(\frac{1}{T_c\,(x,t)} - \frac{1}{T_{ref}}\right)\right], \tag{4.9}$$

where E_a ranges between 30 - 60 kJ/mol. Here, the average activation energy for the first 24 hours after placement was taken as 31.9 kJ/mol [3].

Table 4.1: Density ρ and specific heat c_p of cement paste, ASTM quartz sand, MPCM24D, and PCM35CP.

Material	**Subscript**	ρ (kg/m^3)	c_p (J/kg K)	Ref.
Cement paste	m	1965	1530	[37]
ASTM quartz sand	q	2650	745	[36]
MPCM24D	pcm,1	900	$c_{pcm,1}(T)$	[23]
PCM35CP	pcm,2	825	$c_{pcm,2}(T)$	

4.5 Constitutive relationships

Table 4.1 summarizes the density and specific heat capacity of cement paste, ASTM standard quartz sand, MPCM24D and PCM35CP used in the numerical simulations. The MPCM24D's latent heat of fusion h_{sf} was 160 kJ/kg with melting temperature $T_{pc} = 24°$C, and phase change temperature window $\Delta T_{pc} \approx 8°$C [23]. The latent heat of fusion h_{sf} of PCM35CP was 187 kJ/kg with melting temperature $T_{pc} = 35°$C, and phase change temperature window $\Delta T_{pc} \approx 2°$C. Equation (2.3) was used to predict the PCM's specific heat capacity as a function of temperature based on $c_{p,pcm,s}$, T_{pc}, ΔT_{pc}, and h_{sf} for each microencapsulated PCM considered. The effective thermal conductivity k_{eff} shown in Table 4.2 corresponds to that of mortar and MPCM24D-mortar composites aged for 28 days and measured experimentally using the guarded hot-plate method [22]. Here, the mortar and PCM-mortar composite thermal conductivities were assumed to be independent of aging time, as suggested from the literature [3]. In addition, because MPCM24D and PCM35CP consisted of similar materials (paraffin core within a melamine-formaldehyde shell), the effective thermal conductivity k_{eff} of PCM35CP-mortar composite was considered to be the same as that of MPCM24D-mortar composite, for given PCM and quartz sand volume fractions.

The water bath temperature T_w was taken as the measured time-averaged constant temperature $T_w = (T_{10} + T_{11})/2 \approx 20.3°$C. The initial temperature of the composite $T_c(x, 0)$ and steel plate $T_s(x, 0)$ were taken as room temperature T_{room} measured for each experiment and

Table 4.2: Effective thermal properties k_{eff} and $(\rho c_p)_{eff}(T)$ of each PCM-mortar composite specimen used in numerical simulation.

Specimen	ϕ_m	ϕ_{pcm}	ϕ_q	k_{eff} (W/m K) [22]	$(\rho c_p)_{eff,s}$ (MJ/m^3 K)	$(\rho c_p)_{eff,high}$ (MJ/m^3 K)
1	0.45	0	0.55	1.77 ± 0.27	2.439	2.439
2	0.45	0.10	0.45	1.46 ± 0.22	2.412	4.212
3	0.45	0.10	0.45	1.46 ± 0.22	2.398	10.11
4	0.45	0.20	0.35	1.27 ± 0.19	2.357	17.78

equal to about 25°C.

Finally, after 28 days, cement-water hydration reached completion and heat generation was no longer significant. Hence, the temperature evolution within the mortar section reached a periodic steady state. Then, the convective heat transfer coefficients h_∞ at the top surface of the composite and h_w at the bottom surface of the steel plate were evaluated by least square fitting of the measured periodic steady state temperature $T_{exp}(x_j, t_i)$ and predicted periodic steady state temperature $T_c(x_j, t_i)$ of the composite sections on the 30th day. The objective function was expressed as,

$$f(h_\infty, h_w) = \sum_{j=1}^{N_T} \sum_{i=1}^{N_t} \left[T_{\exp}\left(x_j, t_i\right) - T_c\left(x_j, t_i\right)\right]^2 \tag{4.10}$$

where $j \in [1, N_T]$ corresponds to each of the $N_T = 10$ thermocouples, while $i \in [1, N_t]$ corresponds to the temporal measurements acquired during $N_t = 2880$ time steps every 30 s during the course of one day of experiment. The convective heat transfer coefficients were estimated to be $h_\infty = 25$ W/m^2 K and $h_w = 18$ W/m^2 K.

4.6 Method of solution

The transient 1D governing Equations (4.1) and (4.2) for $T_c(x, t)$ and $T_s(x, t)$ were solved along with the corresponding boundary and initial conditions Equations (4.3) to (4.8) using

a semi-implicit finite difference method [36]. The solution was considered to be numerically converged when the resulting composite temperature $T_c(x,t)$ at any time t or spatial location x differed by no more than 1% after reducing the nodal spacing Δx and the time step Δt by a factor of 2. A nodal spacing $\Delta x = 3$ mm and time step $\Delta t = 30$ s were sufficient to achieve a numerically converged solution.

CHAPTER 5

Results and discussion

5.1 Effect of inclusions and admixtures on hydration

To assess the effect of PCM, quartz sand inclusions, and water-reducing admixture (WRA) on cement hydration, isothermal calorimetry measurements of heat generation rate $\dot{q}_g(t)$ in mortar samples with compositions summarized in Table 3.2 were carried out at $T_{ref} = 25°\text{C}$. Figure 5.1a shows the measured heat generation rate $\dot{q}_g(t_{eq})$ for the six different mortar compositions. Figure 5.1b shows the corresponding measured total thermal energy $Q_g(t_{eq})$ in (J/g) released during cement hydration and expressed as

$$Q_g\left(t_{eq}\right) = \int_0^{t_{eq}} \dot{q}_g\left(t_{eq}\right) \mathrm{d}t_{eq}. \tag{5.1}$$

It is evident that the PCM and quartz inclusions had no significant influence on $\dot{q}_g(t_{eq})$ and $Q_g(t_{eq})$. However, the addition of WRA delayed the heat generation peak from 6 hours to 9 hours and decreased the total thermal energy $Q_g(t_{eq})$ released in the first 12 hours. These results were consistent with previous studies [3, 27].

5.2 Experimental temperature profiles of PCM-mortar composites

Figure 5.2 plots the temporal evolution of local composite temperature $T_c(x, t)$ at various spatial locations from the bottom ($x = 0$) to the top ($x = L_c$) of the four PCM-mortar specimens with compositions summarized in Table 3.1. The maximum temperature was always reached near the middle of the test section around 12 to 17 hours after placement. Figure 5.2b establishes that adding 10 vol.% MPCM24D into the mortar did not reduce

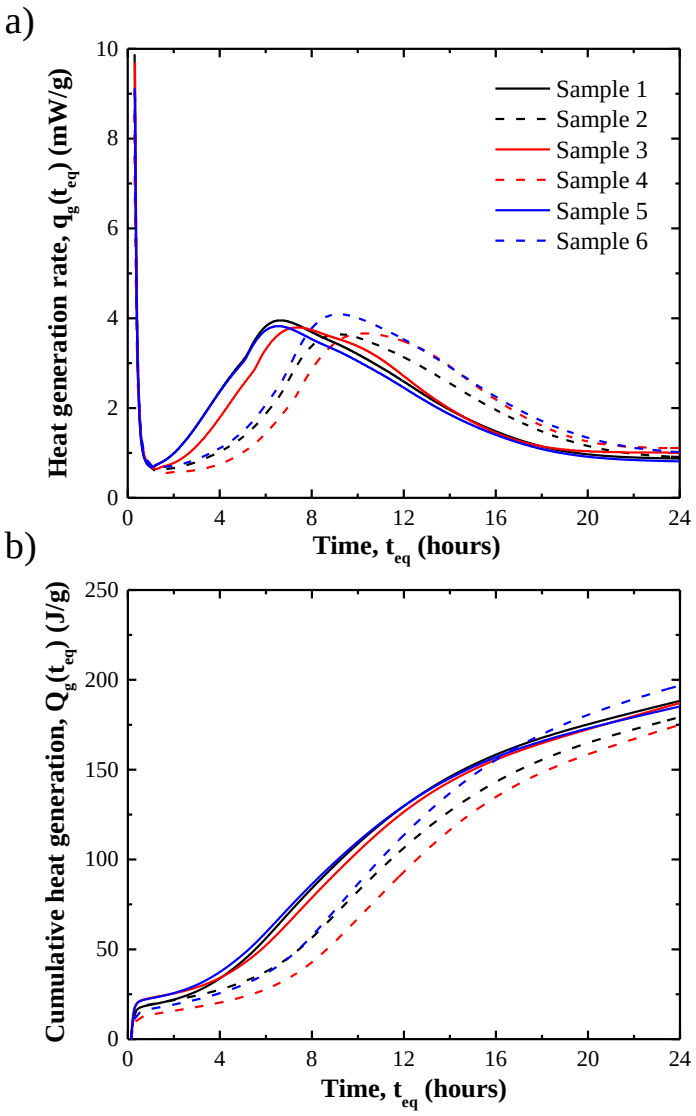

Figure 5.1: (a) Experimentally measured isothermal heat generation rate $\dot{q}_g(t_{eq})$ per unit mass of cement at 25°C for different sample compositions listed in Table 3.2. (b) Corresponding isothermal thermal energy $Q_g(t_{eq})$ released per unit mass of cement.

its early-age temperature compared with the plain mortar section (Figure 5.2a). Instead, the temperature rise was delayed from around 12 hours to around 14 hours after placement and the maximum temperature increased from 51°C to 54°C. These observations could be attributed to the fact that (i) WRA (1.5%) was added to the PCM-mortar composite to ensure its workability but also delayed the exothermic hydration reactions, (ii) the PCM's latent heat was not exploited because the MPCM24D had already melted prior to the start of the experiment since the initial temperature of the mortar was around 25°C (Figure 5.2b), and (iii) the effective thermal conductivity of the composite decreased as MPCM24D was added thus preventing heat dissipation to the surrounding. However, Figure 5.2c indicates that adding 10 vol.% PCM35CP reduced the maximum temperature from 51°C to 47°C. It also features a plateau after around 8 hours at temperature around 35°C caused by the melting of the PCM. Finally, Figure 5.2d established that adding 20 vol.% PCM35CP further reduced the maximum temperature to 42°C and delayed the temperature peak further to around 17 hours after placement because more WRA (2.0%) was added compared with 10 vol.% PCM35CP addition. These results indicate that adding PCM with phase change temperature of 35°C can reduce the temperature rise of the PCM-mortar composite by nearly 10°C thus reducing the risk of early-age thermal cracking.

5.3 Experimental rate of temperature change in PCM-mortar composites

Figures 5.3 plots the local rate of temperature change at different spatial locations from the bottom ($x = 0$) to near the top ($x = 8L_c/9$) for (a) pure mortar, (b) 10 vol.% MPCM24D-mortar composite, (c) 10 vol.% PCM35CP-mortar composite, and (d) 20 vol.% PCM35CP-mortar composite (Table 3.1). Note that the local rate of temperature change dT_9/dt measured on the top surface ($x = L_c$) was not shown because it fluctuated substantially and unrealistically over time as it was measured near the air/PCM-mortar composite section interface. The highest rate of temperature change was systematically reached near the middle of the test section around 6 to 10 hours after placement. The lowest rate of temperature

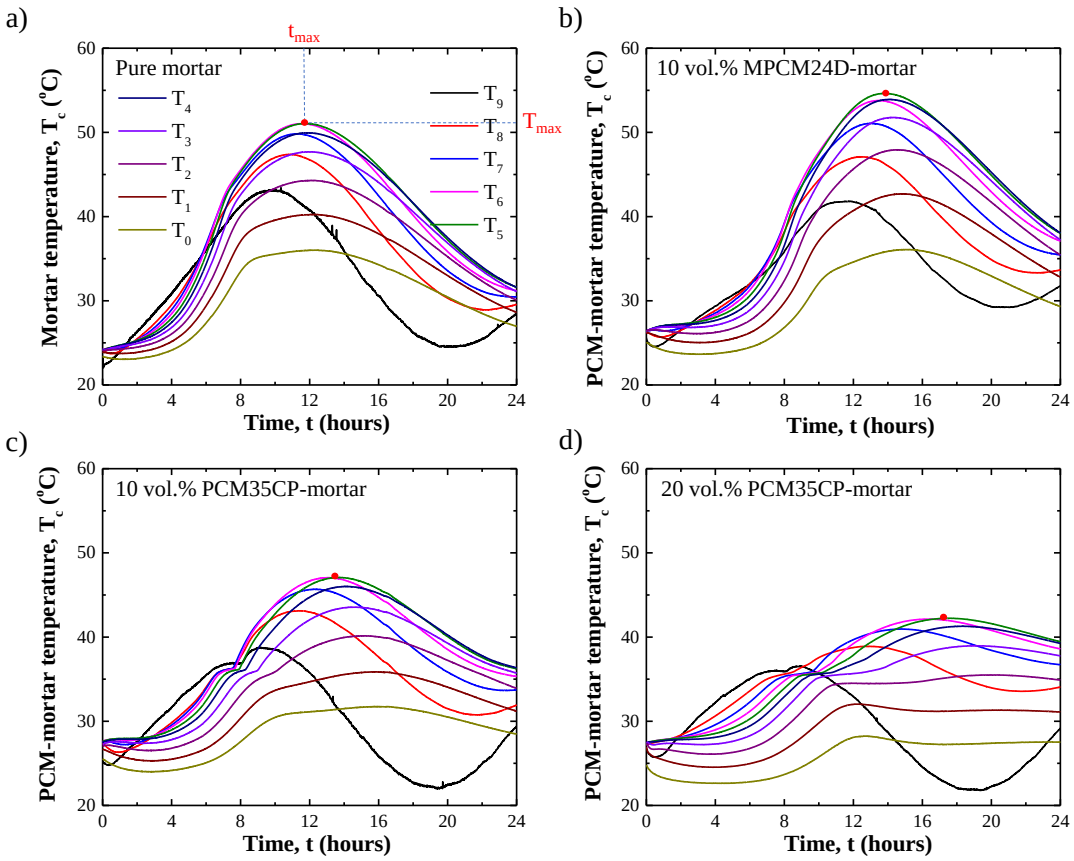

Figure 5.2: Experimentally measured temperature as a function of time at ten different locations along the vertical centerline of each PCM-mortar composite specimen during the first 24 hours after placement for (a) pure mortar, (b) 10 vol.% MPCM24D-mortar composite, (c) 10 vol.% PCM35CP-mortar composite, and (d) 20 vol.% PCM35CP-mortar composite. See Table 3.1 for composition.

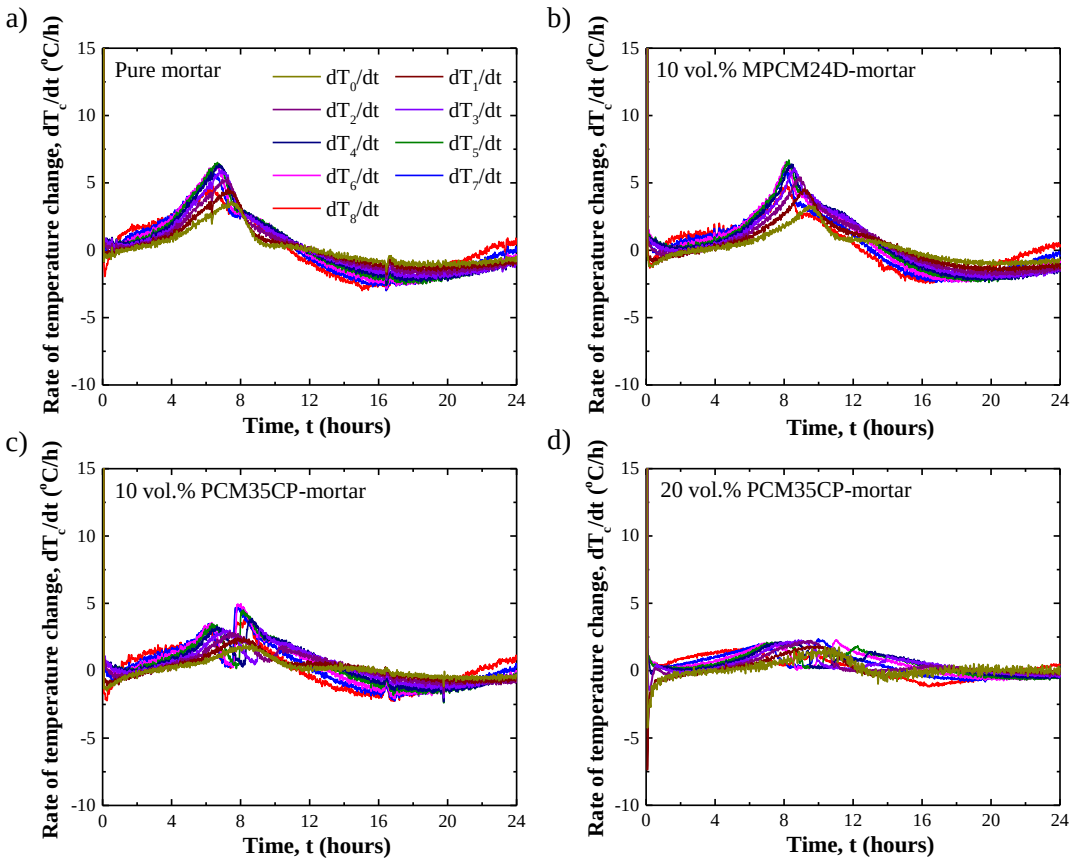

Figure 5.3: Experimentally measured rate of temperature change as a function of time at nine different locations along the vertical centerline of each PCM-mortar composite specimen during the first 24 hours after placement for (a) pure mortar, (b) 10 vol.% MPCM24D-mortar composite, (c) 10 vol.% PCM35CP-mortar composite, and (d) 20 vol.% PCM35CP-mortar composite. See Table 3.1 for composition.

change ($dT_c/dt < 0$), which corresponded to the highest cooldown rate, was always reached near the top surface of the test sections about 14 hours after placement where cooling was the strongest. The cooldown rate decreased when the location of measurement was closer to the bottom surface. Figures 5.3c and 5.3d establish that adding PCM35CP reduced both temperature rise rate and the cooldown rate within PCM-mortar composite section in the first 24 hours after placement except near the top surface. This effect was stronger with increasing PCM loading. These results establish that adding PCM with proper phase change temperature and dosage can reduce the cooldown rate of PCM-mortar composite considerably thus reducing both the risk of early-age cracking due to shrinkage and the depth of crack [25].

5.4 Comparison between experiments and numerical simulations

Figures 5.4 and 5.5 respectively show the numerically simulated temporal evolution of temperature and the corresponding rate of temperature change along the centerline of the pavement section at the same set of locations as in the experiments. Comparison with experimental results shown in Figures 5.2 and 5.3 indicate that numerical simulations agree very well qualitatively and quantitatively with experimental data. For example, the numerically predicted maximum temperature and highest rate of temperature change were reached near the middle of the test section at the same time as that observed experimentally. In addition, Figure 5.6 compares the experimentally measured and numerically predicted maximum temperature T_{max} versus the corresponding time t_{max} for the four PCM-mortar composite specimens of interest (Table 3.1). The experimental uncertainty in the maximum temperature T_{max} was $\pm$ 1°C and the corresponding uncertainty in t_{max} was around $\pm$ 1 hour. Figure 5.6 shows good agreement between experimental measurements and numerical predictions for both T_{max} and t_{max}. The discrepancies were likely caused by the uncertainties in the effective thermal properties k_{eff} and $(\rho c_p)_{eff}$ used in the simulations.

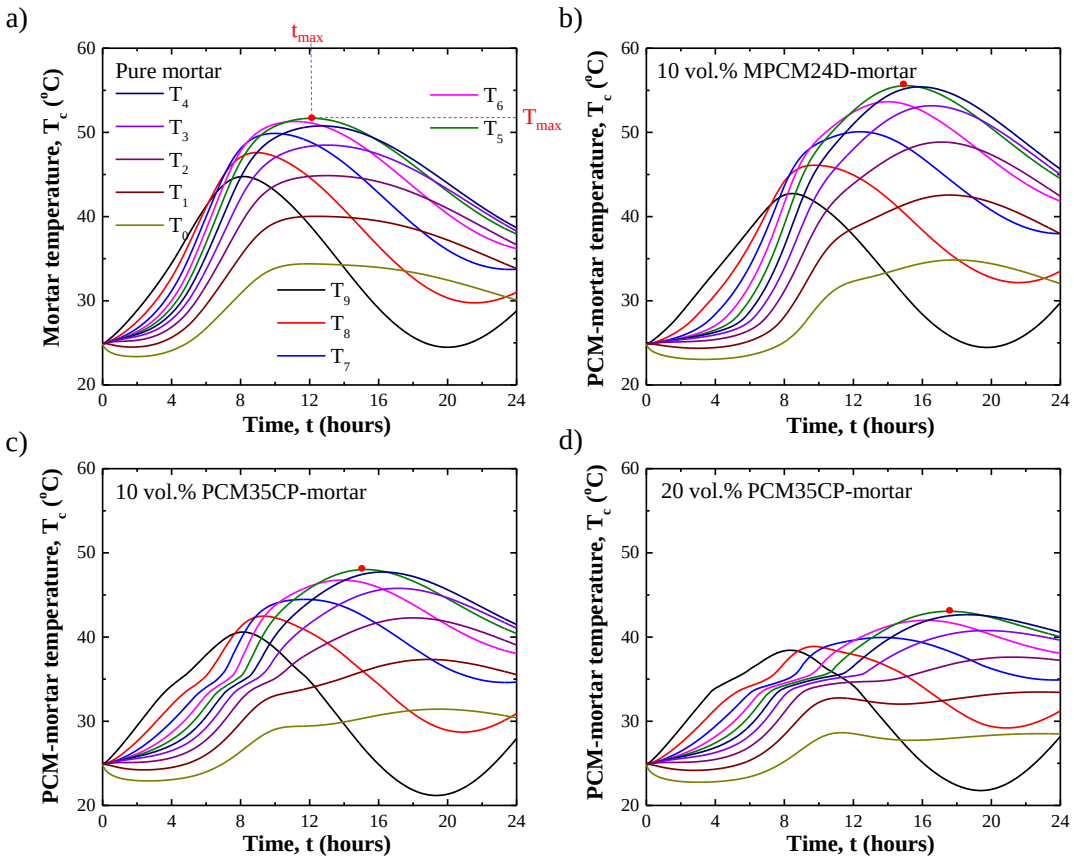

Figure 5.4: Numerically predicted temperature as a function of time at ten different locations along the vertical centerline of each PCM-mortar composite specimen during the first 24 hours after placement for (a) pure mortar, (b) 10 vol.% MPCM24D-mortar composite, (c) 10 vol.% PCM35CP-mortar composite, and (d) 20 vol.% PCM35CP-mortar composite. See Table 3.1 for composition.

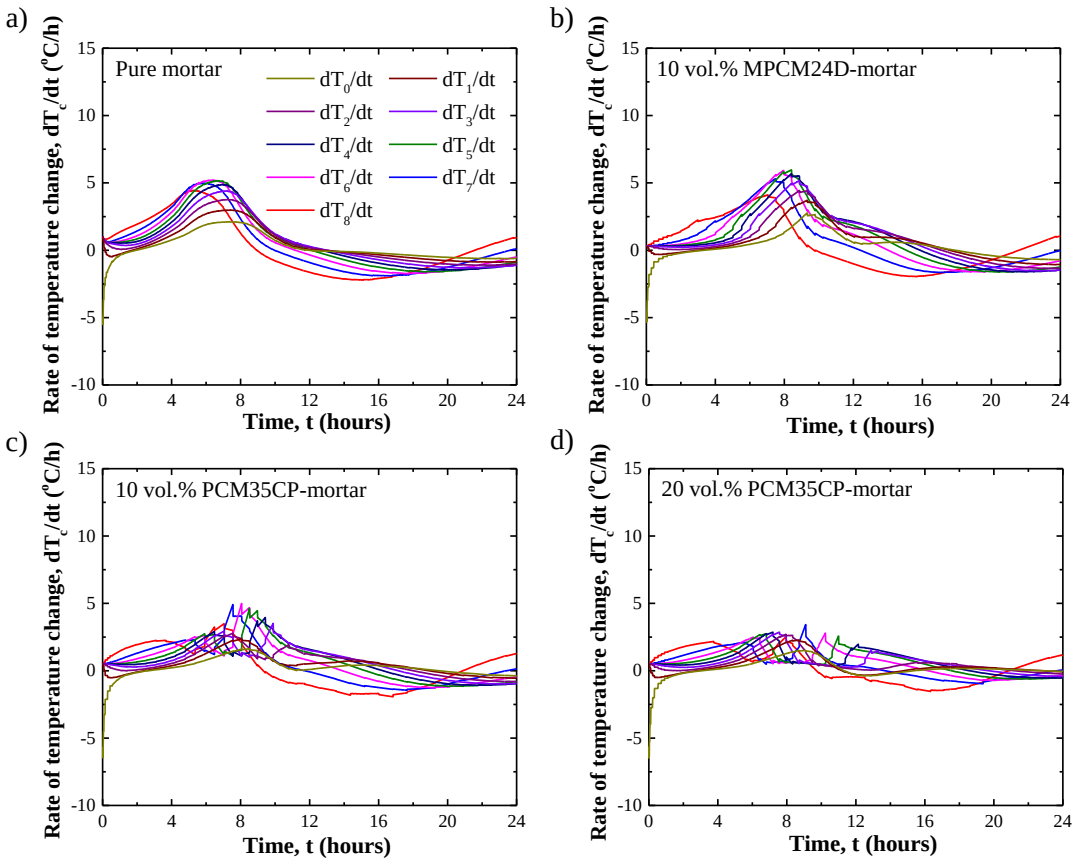

Figure 5.5: Numerically predicted rate of temperature change as a function of time at nine different locations along the vertical centerline of each PCM-mortar composite specimen during the first 24 hours after placement for (a) pure mortar, (b) 10 vol.% MPCM24D-mortar composite, (c) 10 vol.% PCM35CP-mortar composite, and (d) 20 vol.% PCM35CP-mortar composite. See Table 3.1 for composition.

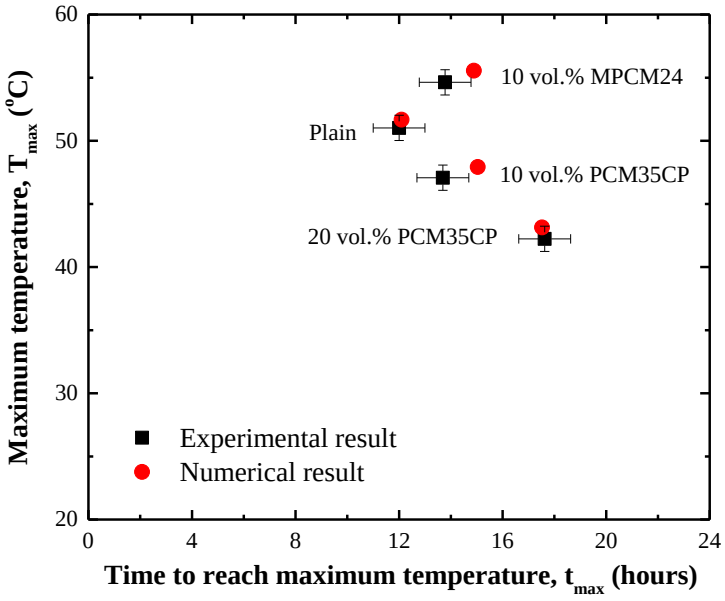

Figure 5.6: Comparison of experimentally measured and numerically predicted maximum temperature T_{max} and corresponding time t_{max} within the PCM-mortar composite sections during the first 24 hours after placement.

Figure 5.7 shows (a) the experimental measurements and (b) the numerical predictions of the local temperature T_3 at $x = 3L_c/9$ and T_5 at $x = 5L_c/9$ and the corresponding rates of temperature change dT_3/dt and dT_5/dt for 20 vol.% PCM35CP-mortar composite. Both plots feature a common plateau after around 8 hours when temperature approached the PCM melting temperature of 35°C. In other words, dT_c/dt approached 0 when PCM was melting in the temperature range $T_{pc} \pm \Delta T_{pc}/2$. Consequently PCM melting helped reduce the temperature rise and damp the rate of temperature change of concrete at early ages. Overall, the 1D transient thermal model developed performed well and can be used to accurately predict temperature development and cooldown rate within early-age concrete pavements.

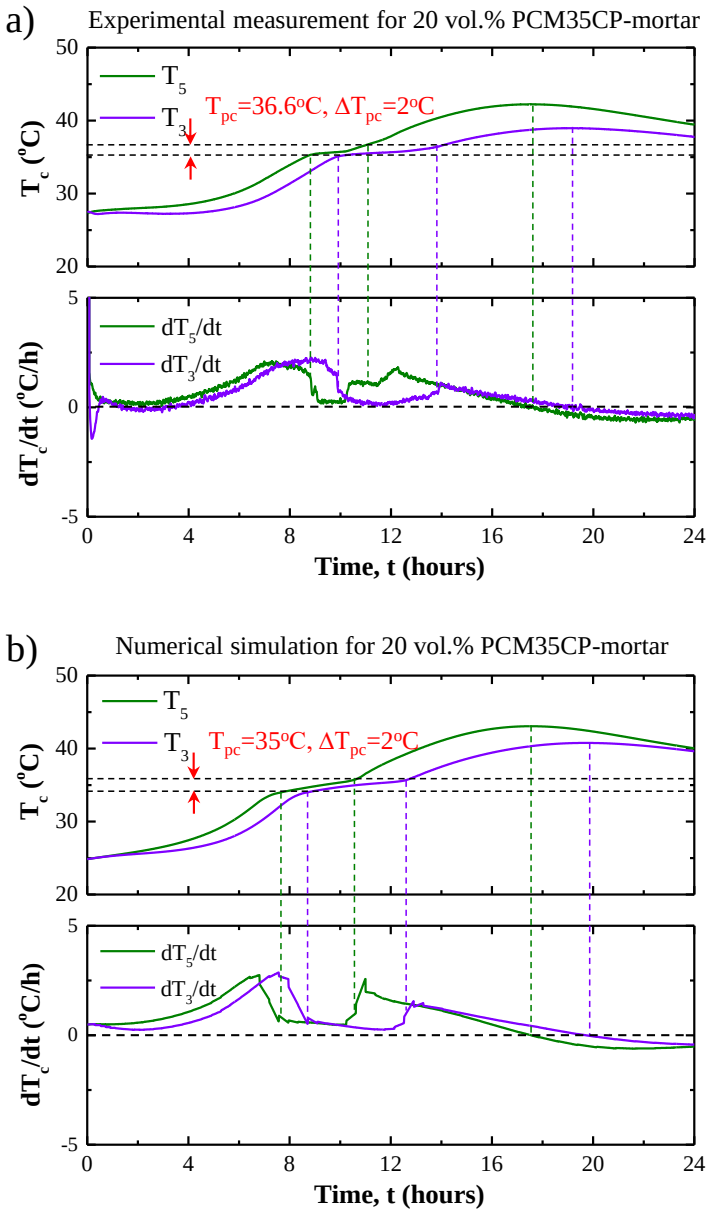

Figure 5.7: (a) Experimentally measured and (b) numerically predicted temperature and corresponding rate of temperature change as functions of time at $3L_c/9$ and $5L_c/9$ of 20 vol.% PCM35CP-mortar composite.

5.5 Parametric study

5.5.1 Effect of PCM melting temperature and melting temperature window

Figure 5.8 plots (a) the maximum temperature T_{max} and (b) the maximum cooldown rate $(-dT_c/dt)_{max}$ within 20 vol.% PCM-mortar composite section as functions of the PCM melting temperature T_{pc} ranging from 26°C to 40°C. Different values of PCM melting temperature window ΔT_{pc} ranging from 2°C to 8°C were also considered. The PCM's latent heat of fusion h_{sf} is 187 kJ/kg. The environmental temperature setting was still the same as that applied in the experiment and numerical simulation. Also, the maximum temperature and maximum cooldown rate within a pure mortar section exposed to the same temperature conditions are shown in the plots as references. In Figure 5.8a, the maximum temperature T_{max} does not show a significant dependence on the melting temperature window ΔT_{pc} as long as the temperature window is fully encompassed within the placement temperature T_{room} and minimum temperature T_{min} of PCM-mortar composite section when the composite reaches the highest temperature at its early ages. When the PCM melting temperature T_{pc} and melting temperature window ΔT_{pc} satisfy the following correlation

$$T_{room} + \frac{\Delta T_{pc}}{2} \leq T_{pc} \leq T_{\min} - \frac{\Delta T_{pc}}{2}, \tag{5.2}$$

all PCM within PCM-mortar composite will melt during the cement hydration process, thus giving the greatest reduction in the temperature rise of PCM-mortar composite at its early ages.

Figure 5.8b shows no significant improvement on maximum cooldown rate $(-dT_c/dt)_{max}$ by adding PCMs comparing to that of pure mortar. The maximum cooldown rate always occurs on the top surface of the PCM-mortar composite as it is exposed to the environment directly, the rate of temperature change is strongly related to the ambient temperature T_∞ and convective heat transfer coefficient h_∞ on the top surface rather than the thermal properties of the PCM-mortar composite studied. However, it can be seen from Figure 5.3 that cooldown rates were damped after 12 hours as more PCM was added except for that of top surface, which can still reduce the risk of early-age cracking due to shrinkage when

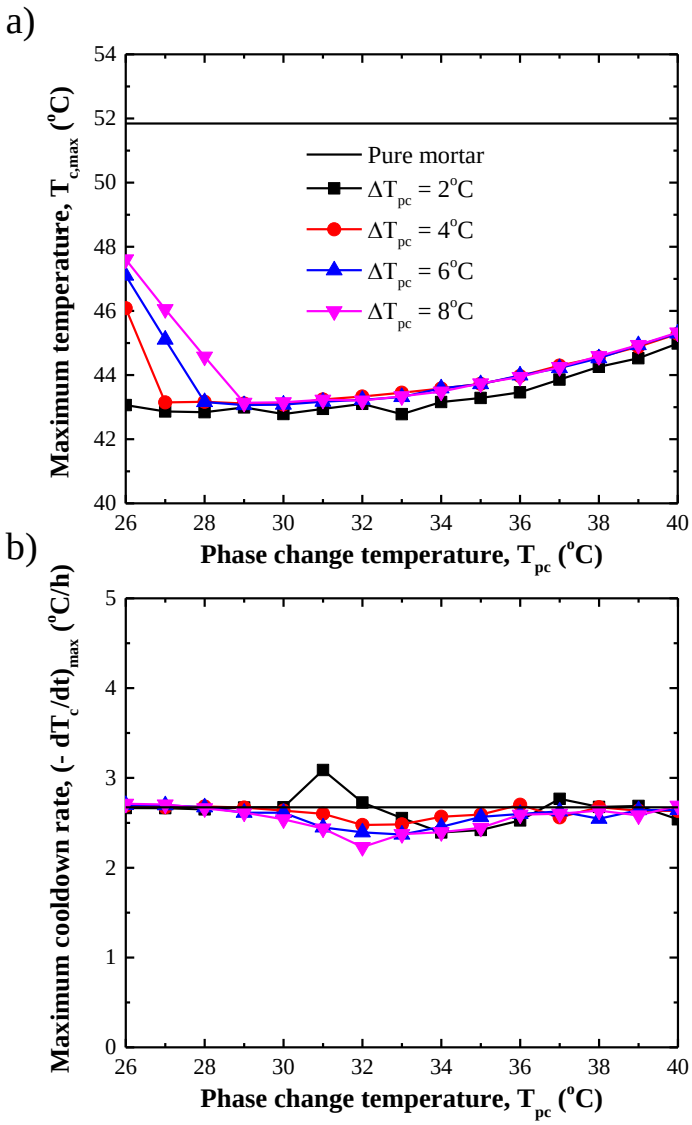

Figure 5.8: The effect of PCM's phase change temperature T_{pc} and phase change temperature window ΔT_{pc} on (a) the maximum temperature T_{max} and (b) the maximum cooldown rate $(-dT_c/dt)_{max}$ within a PCM-mortar composite placed under the experimental temperature setting. The PCM volume fraction was $\phi_{pcm} = 0.2$ and its latent heat of fusion was $h_{sf} =$ 187 kJ/kg.

concrete cools down as the original temperature of top surface is not that high as Figure 5.2 suggests.

5.5.2 Effect of PCM volume fraction and latent heat of fusion

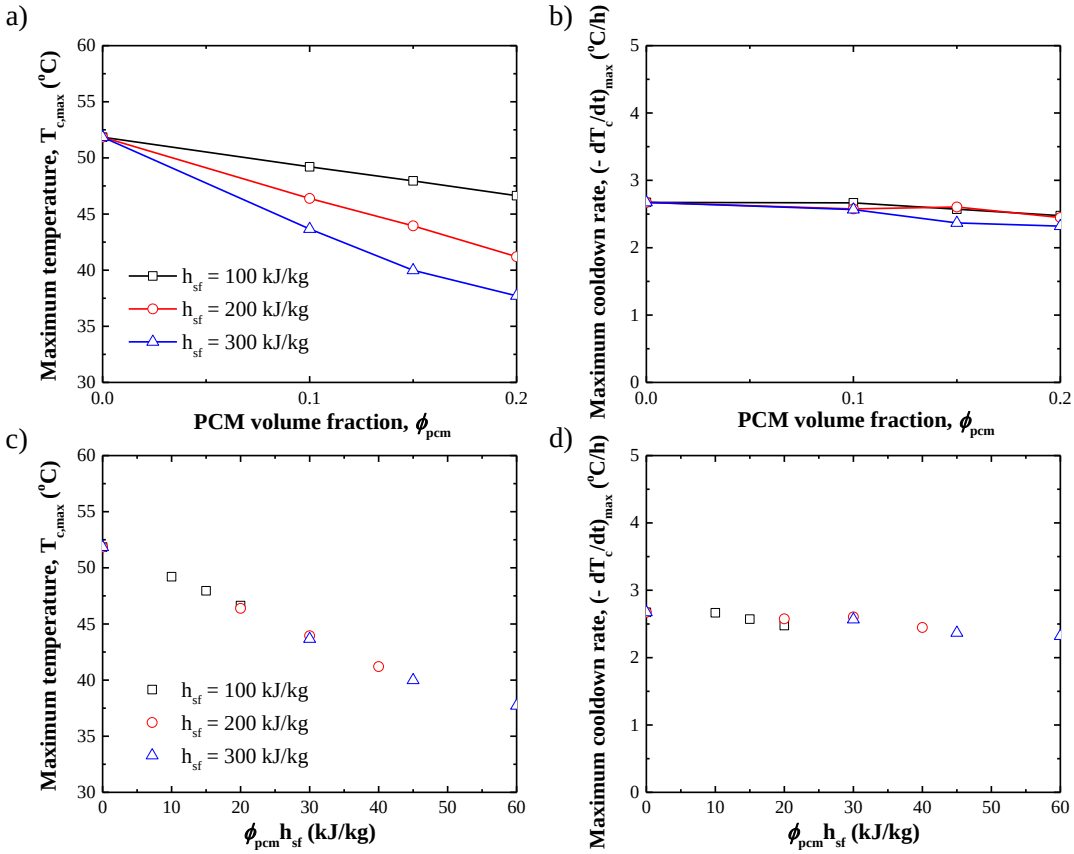

Figure 5.9: The effect of PCM volume fraction ϕ_{pcm} and PCM latent heat of fusion h_{sf} on (a) the maximum temperature T_{max} and (b) the maximum cooldown rate $(-dT_c/dt)_{max}$ within a PCM-mortar composite placed under the experimental temperature setting. The effect of the product $\phi_{pcm}h_{sf}$ on (c) the maximum temperature T_{max} and (d) the maximum cooldown rate $(-dT_c/dt)_{max}$ within a PCM-mortar composite placed under the experimental temperature setting. The PCM's phase change temperature was $T_{pc} = 35°C$ and the phase change temperature window was $\Delta T_{pc} = 2°C$.

Figure 5.9 plots (a) the maximum temperature T_{max} and (b) the maximum cooldown rate $(-dT_c/dt)_{max}$ within a PCM-mortar composite section as functions of the PCM volume fraction ϕ_{pcm} and its latent heat of fusion h_{sf}. Figure 5.9a illustrates that the maximum temperature decreased with increasing PCM volume fraction or PCM latent heat.

Figure 5.9 also shows (c) the maximum temperature T_{max} and (d) the maximum cooldown rate $(-dT_c/dt)_{max}$ within a PCM-mortar composite section as functions of product $\phi_{pcm}h_{sf}$, which represents the total latent heat storage capacity of the PCM-mortar composite. It establishes that the reduction in temperature contributed by PCM addition only depends on this product, rather than ϕ_{pcm} or h_{sf} individually. It should be noted that it would not be the case if the effective thermal conductivity of the PCM-mortar composite was allowed to change with different PCM dosage. Also, since too much addition of PCMs can negatively impact the mechanical properties of cementitious composites [38, 39], it is beneficial to increase the amount of latent heat storage in the composite by increasing PCM latent heat h_{sf} rather than ϕ_{pcm}, which is also suggested by Šavija *et al.* [24] and Young *et al.* [3]. Figure 5.9b and 5.9d still show no significant improvement on maximum cooldown rate $(-dT_c/dt)_{max}$ by adding PCMs comparing to that of pure mortar.

CHAPTER 6

Conclusion

This study established experimentally the benefits of adding microencapsulated PCMs into concrete pavement to minimize early-age cracking. It demonstrated that adding microencapsulated PCMs into cementitious composites with melting temperature above the initial temperature can reduce the temperature rise caused by heat generation from cement hydration and the cooldown rate during the first 24 hours after placement despite the delay in cement hydration caused by WRA addition and the adverse thermally insulating effect of the PCM microcapsules. Hence, adding microencapsulated PCMs could be an effective method for mitigating the risk of early-age thermal cracking. A 1D transient thermal model was also developed using the heat generation rate measured by isothermal calorimetry based on the time-temperature equivalent age method. Good qualitative and quantitative agreements were observed between experimentally measured and numerically predicted temperature evolutions within the different mortar sections. Thus, the 1D thermal model with the thermophysical properties of PCM-mortar composite and heat generation rate associated with cement hydration can be used to predict temperature development within fresh concrete pavements.

REFERENCES

[1] Pavia Systems Inc. Close-up of early age crack. `http://www.pavementinteractive.org/early-age-behavior/`, 2012. [Online; accessed May 31, 2018].

[2] B. Zhu. *Thermal Stresses and Temperature Control of Mass Concrete*. Butterworth-Heinemann, Oxford, UK, 2013.

[3] B.A. Young, G. Falzone, Z. She, A.M. Thiele, Z. Wei, N. Neithalath, G. Sant, and L. Pilon. Early-age temperature evolutions in concrete pavements containing microencapsulated phase change materials. *Construction and Building Materials*, 147:466–477, 2017.

[4] D.P. Bentz. A review of early-age properties of cement-based materials. *Cement and Concrete Research*, 38(2):196–204, 2008.

[5] S.N. AL-Saadi and Z.J. Zhai. Modeling phase change materials embedded in building enclosure: A review. *Renewable and Sustainable Energy Reviews*, 21:659–673, 2013.

[6] D.P. Bentz, M.R. Geiker, and K.K. Hansen. Shrinkage-reducing admixtures and early-age desiccation in cement pastes and mortars. *Cement and Concrete Research*, 31(7):1075–1085, 2001.

[7] M. Şahmaran, M. Lachemi, K. MA Hossain, and V.C. Li. Internal curing of engineered cementitious composites for prevention of early age autogenous shrinkage cracking. *Cement and Concrete Research*, 39(10):893–901, 2009.

[8] K.L. Lees and K.R. Edwars. Cryogenic cooling of concrete, June 8, 1971. US Patent 3,583,172.

[9] D.P. Bentz and R. Turpin. Potential applications of phase change materials in concrete technology. *Cement and Concrete Composites*, 29(7):527–532, 2007.

[10] F. Fernandes, S. Manari, M. Aguayo, K. Santos, T. Oey, Z. Wei, G. Falzone, N. Neithalath, and G. Sant. On the feasibility of using phase change materials (PCMs) to mitigate thermal cracking in cementitious materials. *Cement and Concrete Composites*, 51:14–26, 2014.

[11] C. Qian, G. Gao, C. Zhu, and Z. Guo. Influence of phase change materials on temperature rise caused by hydration heat evolution of cement-based materials. *Magazine of Concrete Research*, 62(11):789–794, 2010.

[12] C. Qian and G. Gao. Reduction of interior temperature of mass concrete using suspension of phase change materials as cooling fluid. *Construction and Building Materials*, 26(1):527–531, 2012.

[13] V.V. Tyagi and D. Buddhi. PCM thermal storage in buildings: a state of art. *Renewable and Sustainable Energy Reviews*, 11(6):1146–1166, 2007.

[14] L.F. Cabeza, C. Castellon, M. Nogues, M. Medrano, R. Leppers, and O. Zubillaga. Use of microencapsulated PCM in concrete walls for energy savings. *Energy and Buildings*, 39(2):113–119, 2007.

[15] A. Jamekhorshid, S.M. Sadrameli, and M. Farid. A review of microencapsulation methods of phase change materials (PCMs) as a thermal energy storage (TES) medium. *Renewable and Sustainable Energy Reviews*, 31:531–542, 2014.

[16] G. Fang, Z. Chen, and H. Li. Synthesis and properties of microencapsulated paraffin composites with SiO_2 shell as thermal energy storage materials. *Chemical Engineering Journal*, 163(1):154–159, 2010.

[17] A. Arora, G. Sant, and N. Neithalath. Numerical simulations to quantify the influence of phase change materials (PCMs) on the early-and later-age thermal response of concrete pavements. *Cement and Concrete Composites*, 81:11–24, 2017.

[18] ASCE. 2017 Infrastructure Report Card. *American Society of Civil Engineers*, 2017.

[19] A.M. Thiele, A. Kumar, G. Sant, and L. Pilon. Effective thermal conductivity of three-component composites containing spherical capsules. *International Journal of Heat and Mass Transfer*, 73:177–185, 2014.

[20] A.M. Thiele, G. Sant, and L. Pilon. Diurnal thermal analysis of microencapsulated PCM-concrete composite walls. *Energy Conversion and Management*, 93:215–227, 2015.

[21] J.D. Felske. Effective thermal conductivity of composite spheres in a continuous medium with contact resistance. *International Journal of Heat and Mass Transfer*, 47(14):3453–3461, 2004.

[22] A. Ricklefs, A.M. Thiele, G. Falzone, G. Sant, and L. Pilon. Thermal conductivity of cementitious composites containing microencapsulated phase change materials. *International Journal of Heat and Mass Transfer*, 104:71–82, 2017.

[23] A.M. Thiele, Z. Wei, G. Falzone, B.A. Young, N. Neithalath, G. Sant, and L. Pilon. Figure of merit for the thermal performance of cementitious composites containing phase change materials. *Cement and Concrete Composites*, 65:214–226, 2016.

[24] B. Šavija and E. Schlangen. Use of phase change materials (PCMs) to mitigate early age thermal cracking in concrete: Theoretical considerations. *Construction and Building Materials*, 126:332–344, 2016.

[25] B. Klemczak and A. Knoppik-Wróbel. Early age thermal and shrinkage cracks in concrete structures–description of the problem. *Architecture-Civil Engineering-Environment*, 4(2):35–48, 2011.

[26] A. Jayalath, R. San Nicolas, M. Sofi, R. Shanks, T. Ngo, L. Aye, and P. Mendis. Properties of cementitious mortar and concrete containing micro-encapsulated phase change materials. *Construction and Building Materials*, 120:408–417, 2016.

[27] F. Puertas, H. Santos, M. Palacios, and S. Martínez-Ramírez. Polycarboxylate superplasticiser admixtures: effect on hydration, microstructure and rheological behaviour in cement pastes. *Advances in Cement Research*, 17(2):77–89, 2005.

[28] Z. Ge, K. Wang, and Z. Gao. Prediction of pavement concrete strength development, joint sawing, and opening time using FEMLAB. *Journal of Performance of Constructed Facilities*, 26(2):162–169, 2011.

[29] R.C. Tank and N.J. Carino. Rate constant functions for strength development of concrete. *Materials Journal*, 88(1):74–83, 1991.

[30] P.F. Hansen and E.J. Pedersen. Maturity computer for controlled curing and hardening of concrete. *Nordisk Betong*, 1:19–34, 1977.

[31] ASTM Standard. C150/C150M-17 Standard Specification for Portland Cement. *ASTM International, West Conshohocken, PA*, 2017.

[32] ASTM Standard. C192/C192M-16a Standard Practice for Making and Curing Concrete Test Specimens in the Laboratory. *ASTM International, West Conshohocken, PA*, 2016.

[33] ASTM Standard. C778-13 Standard Specification for Standard Sand. *ASTM International, West Conshohocken, PA*, 2013.

[34] ASTM Standard. C1702 Standard Test Method for Measurement of Heat of Hydration of Hydraulic Cementitious Materials Using Isothermal Conduction Calorimetry. *ASTM International, West Conshohocken, PA*, 2015.

[35] ASTM Standard. C494/C494M-17 Standard Specification for Chemical Admixtures for Concrete. *ASTM International, West Conshohocken, PA*, 2017.

[36] T.L. Bergman, A.S. Lavine, F.P. Incropera, and D.P. DeWitt. *Fundamentals of Heat and Mass Transfer, seventh edition*. John Wiley & Sons, New York, NY, 2011.

[37] D.P. Bentz. Transient plane source measurements of the thermal properties of hydrating cement pastes. *Materials and Structures*, 40(10):1073–1080, 2007.

[38] B.A. Young, A.M. Fujii, A.M. Thiele, A. Kumar, G. Sant, E. Taciroglu, and L. Pilon. Effective elastic moduli of core-shell-matrix composites. *Mechanics of Materials*, 92:94–106, 2016.

[39] G. Falzone, G.P. Falla, Z. Wei, M. Zhao, A. Kumar, M. Bauchy, N. Neithalath, L. Pilon, and G. Sant. The influences of soft and stiff inclusions on the mechanical properties of cementitious composites. *Cement and Concrete Composites*, 71:153–165, 2016.